Supporting Information

Peculiar Hydrogen Bonding Behaviour of Water Molecules inside the Aqueous Nanochannels of Lyotropic Liquid Crystals

Konoya Das,[I] Subrahmanyam Sappati[I] and Partha Hazra*[,I,‡]

[I]Department of Chemistry, Indian Institute of Science Education and Research (IISER), Pune. Dr. Homi Bhabha Road, Pashan, Pune, India 411008. Fax: +91 20 2590 8186.

[‡]Centre for Energy Science, Department of Chemistry, Indian Institute of Science Education and Research (IISER), Pune, India 411008.

E-mail: p.hazra@iiserpune.ac.in, Tel: +91 20 2590 8077.

Note S1

Polarized Light Microscopy (PLM).

The PLM images of Ia3d and Pn3m do not exhibit any optical texture, which is characteristic of their highly ordered cubic symmetry. The cubic phases have to thus be distinguished by small angle x-ray scattering experiments.

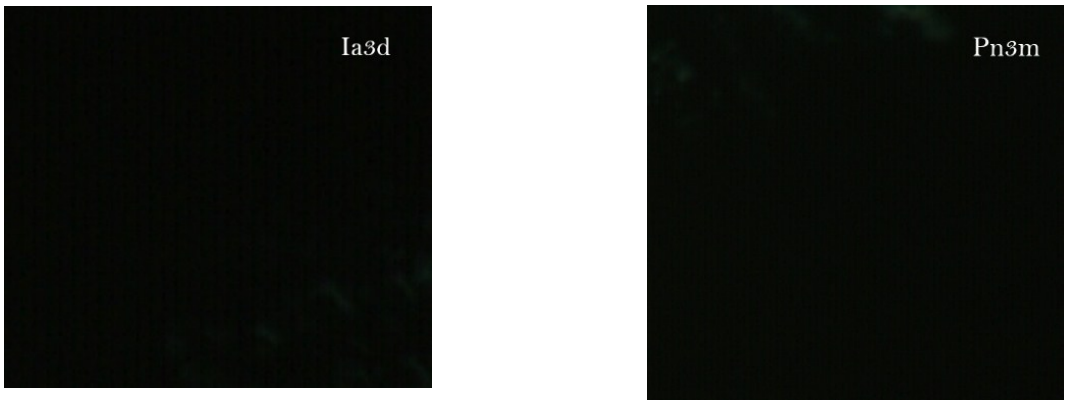

Figure S1. Small-angle X-ray scattering pattern of H_{II}, Pn3m and Ia3d phases at 298 K.

Note S2

Instrumentation.
Small-angle X-ray scattering (SAXS).

The scattering experiment was performed on the line collimated Anton Paar SAXSess mc2 system equipped with a sealed tube copper X-ray source, operating at 40 kV and 50 mA and providing characteristic radiation of wavelength of 1.54 Å. The experiment was carried out in the q range of 0.01 to 0.6 $Å^{-1}$. The sample was filled in the paste cell on a TCS 300-c stage and scanned at room temperature. The scattered data was collected by a 2-D Princeton Instruments PI-SCX:4300 CCD detector. The 1-D scattering profiles were corrected for transmission and background scattering in the Anton Paar SAXSquant softwares.

The observed peak distance ratios for H_{II}, Pn3m and Ia3d are √1:√3, √2:√3:√4:√6:√8 and √6:√8:√14:√16 respectively (Figure S1). The observed peaks match the ideal SAXS diffractograms for these phases, confirming the formation of H_{II}, Pn3m and Ia3d phases.

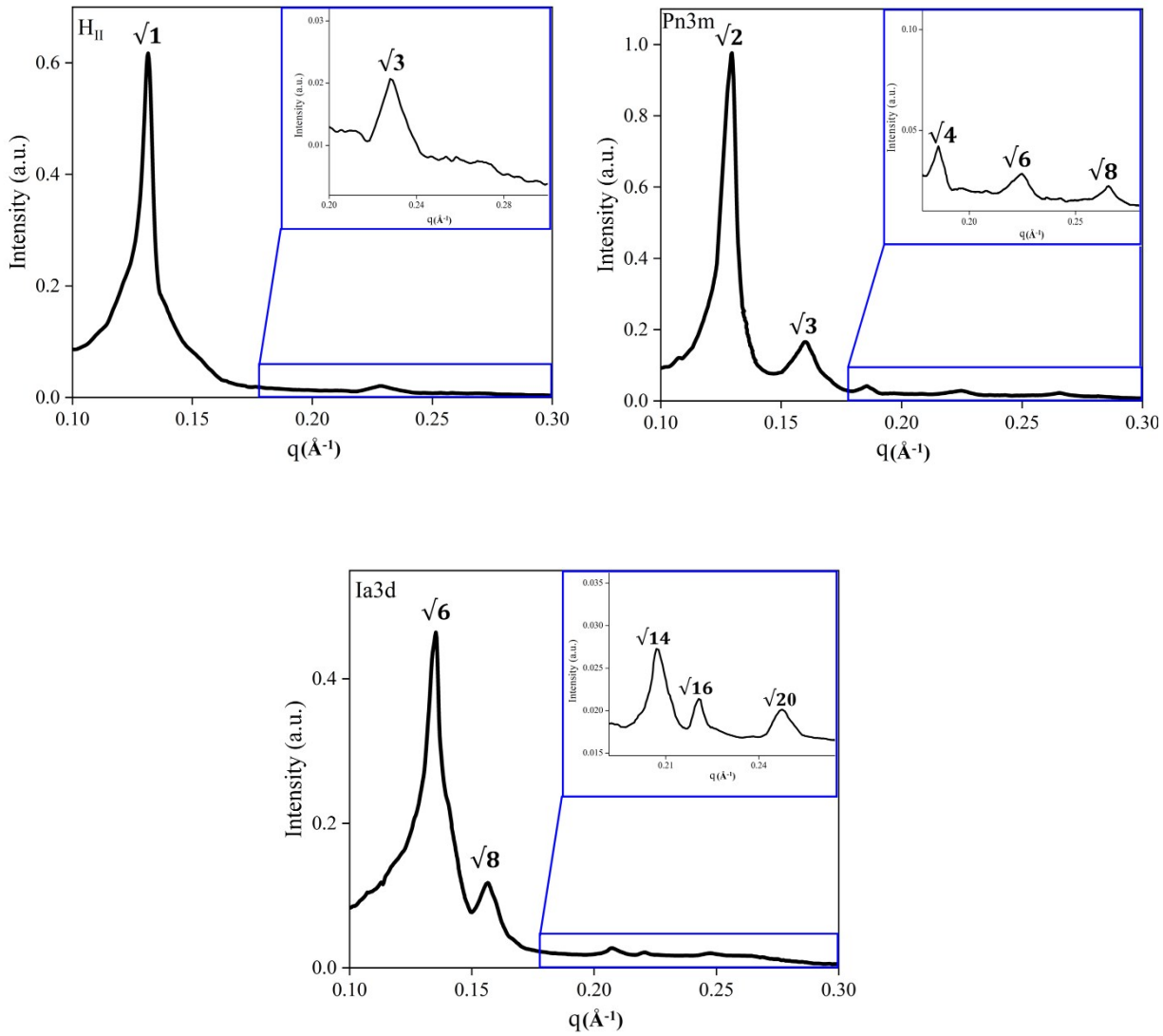

Figure S2. Small-angle X-ray scattering pattern of H_{II}, Pn3m and Ia3d phases at 298 K.

Note S3

Calculation of water channel radius:

The water nanochannel radii of Pn3m, Ia3d and H_{II} LLC phases have been calculated based on the IPMS model.[1, 2]

The bicontinuos cubic phases (Pn3m and Ia3d):

For the two cubic phases Ia3d and Pn3m, we first find out the lipid chain length which is then followed by the calculation of the radius. The lipid chain length (l) can be obtained as,

$$\Phi_{lip} = 2A^* \frac{l}{a} + \frac{4\pi\chi}{3}\left(\frac{l}{a}\right)^3 \quad (1)$$

where, Φ_{lip} is the total volume fraction of the lipid (GMO) used in the binary mixture during the preparation of the phases, A^* is the area of the surface in the unit cell with the lattice parameter equals to unity, χ is the Euler-Poincare characteristic and a is the lattice parameter calculated using the peak position of the highest intensity reflections (110 for Pn3m and 211 for Ia3d phases respectively). Following the calculation of the monolayer thickness value, the radius of the water nanochannels of the cubic phases can be obtained as,

$$R_w = \left(\frac{A^*}{2\pi|\chi|}\right)^{1/2} a - l \quad (2)$$

The values of A^* and χ are 3.091 and -8 respectively for the Ia3d phase and 1.919 and -2 for respectively for the Pn3m phase.[1, 2] The above equation can be written as follows for the cubic phases,

For Ia3d phase, $$R_W = (0.2480)a - l \quad (3)$$

For Pn3m phase, $$R_W = (0.3908)a - l \quad (4)$$

The calculated diameters for the water nanochannels of the synthesised Pn3m and Ia3d phases at 23% volume fraction of water come out to be 2.26 nm and 2.47 nm.

The reverse hexagonal phase (H_{II}):

The radius of the water nanochannel in the H_{II} phase have been calculated by the following equation, [1, 2]

$$R_w = a\left(\frac{\sqrt{3}(1 - \Phi_{lip})}{2\pi}\right)^{1/2} \quad (5)$$

Where, Φ_{lip} is the total volume fraction of the lipid (GMLO) used in the binary mixture during synthesis and a is the lattice parameter, which is obtained from the peak position of the highest intensity (100). The calculated diameter for the synthesised H_{II} phase at 23% volume fraction of water is 2.405 nm.

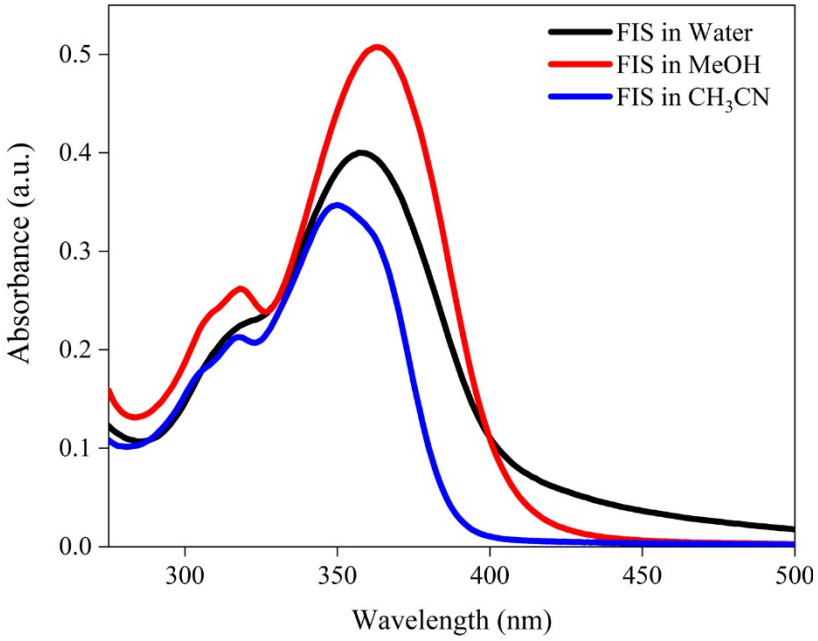

Figure S3. Absorption spectra of FIS in aprotic and protic solvents.

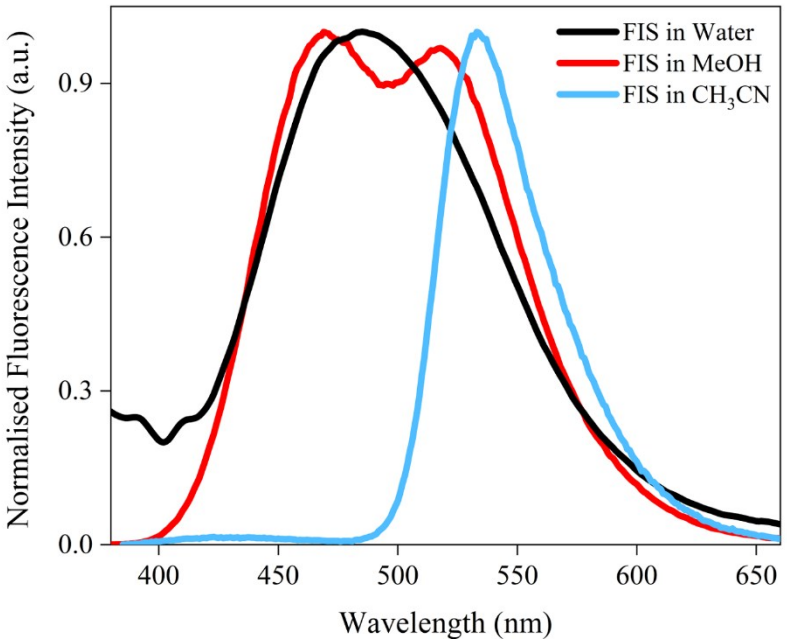

Figure S4. Emission spectra of FIS in different protic and aprotic solvents at λ_{ex} = 360 nm.

Table S1. Kamlet-Taft solvent parameters for some solvents

Solvent	α	β	I_{N*}/I_{T*} (FIS)	I_{N*}/I_{T*} (3HF)
Methanol	0.98	0.66	0.9345	0.442
Ethanol	0.86	0.75	0.387	0.30
Acetonitrile	0.19	0.40	0.018[a]	0.021[a]
Tetrahydrofuran	0.0	0.55	0.014[a]	0.070[a]
Benzene	0.0	0.10	0.011	-

[a]Experimental value

The Kamlet-Taft parameters and values of I_{N*}/I_{T*} for 3HF have been taken from Photochem. Photobiol. Sci., 2018, 17, 923. The dash signifies that only tautomeric emission was present.

The values of I_{N*}/I_{T*} for FIS have been taken from Photochem. Photobiol., 2007, 83, 486.

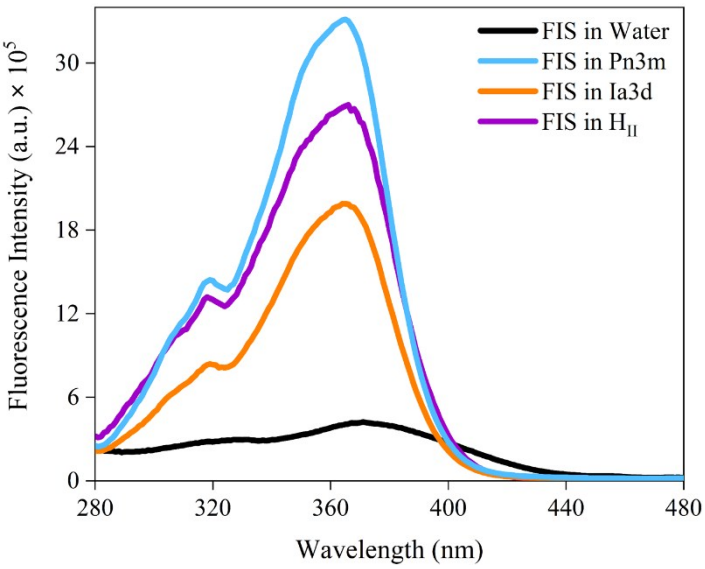

Figure S5. Excitation spectra of FIS in water and LLC phases at λ_{em} = 540 nm.

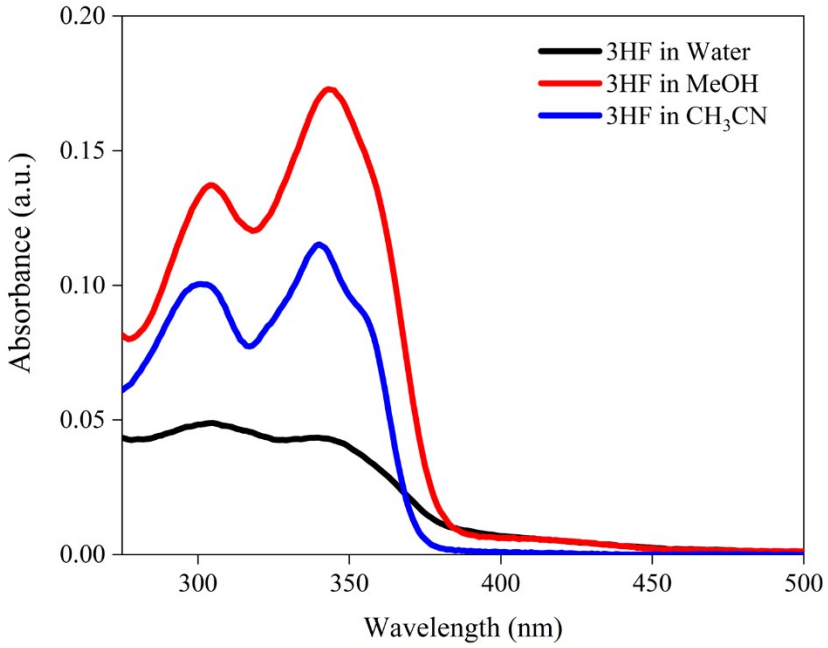

Figure S6. Absorption spectra of 3HF in aprotic and protic solvents.

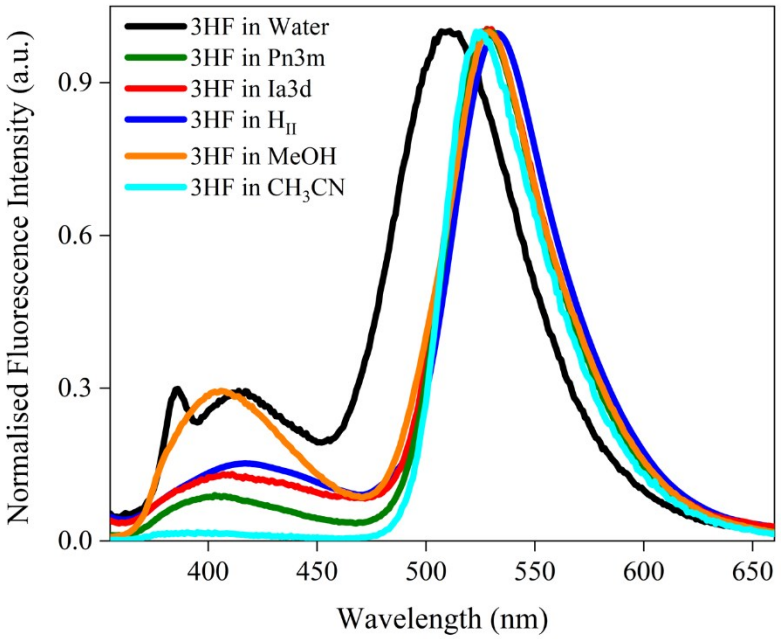

Figure S7. Steady state emission spectra of 3HF in water, methanol, acetonitrile and LLC phases on excitation at 340 nm.

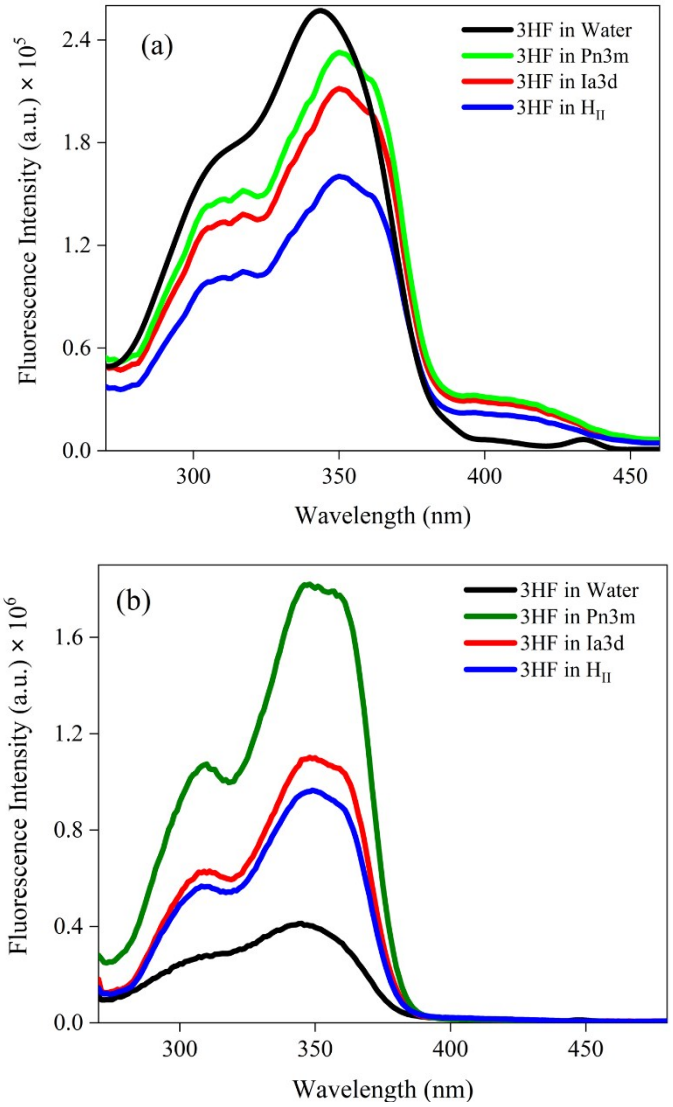

Figure S8. Excitation spectra of 3HF in water and LLC phases at (a) λ_{em} = 480 nm (b) λ_{em} = 530 nm.

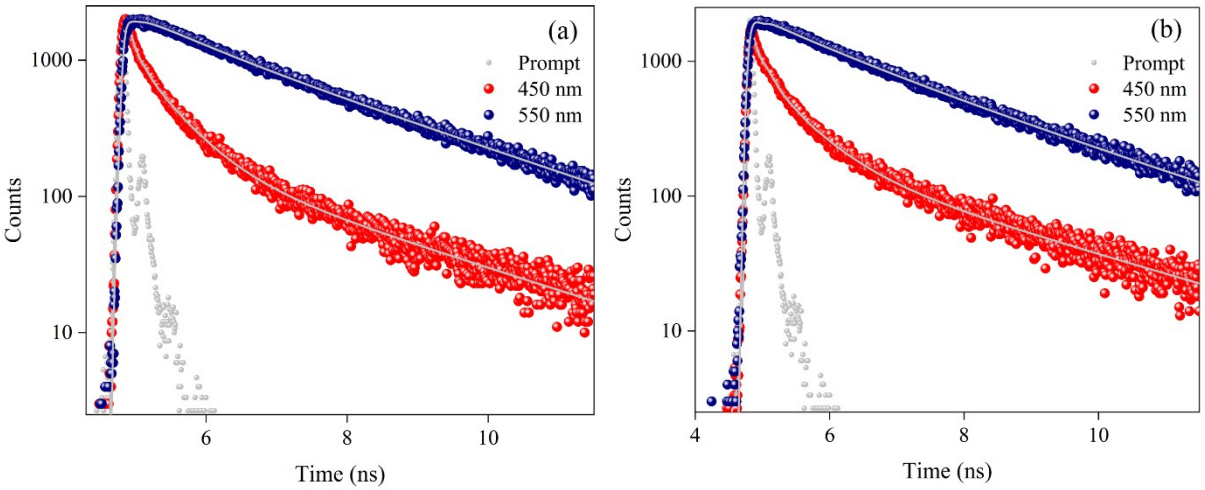

Figure S9. Lifetime decay profiles of FIS in (a) Ia3d and (b) Pn3m LLC phases collected at different emission wavelengths. The solid lines denote the fits of the decay profiles.

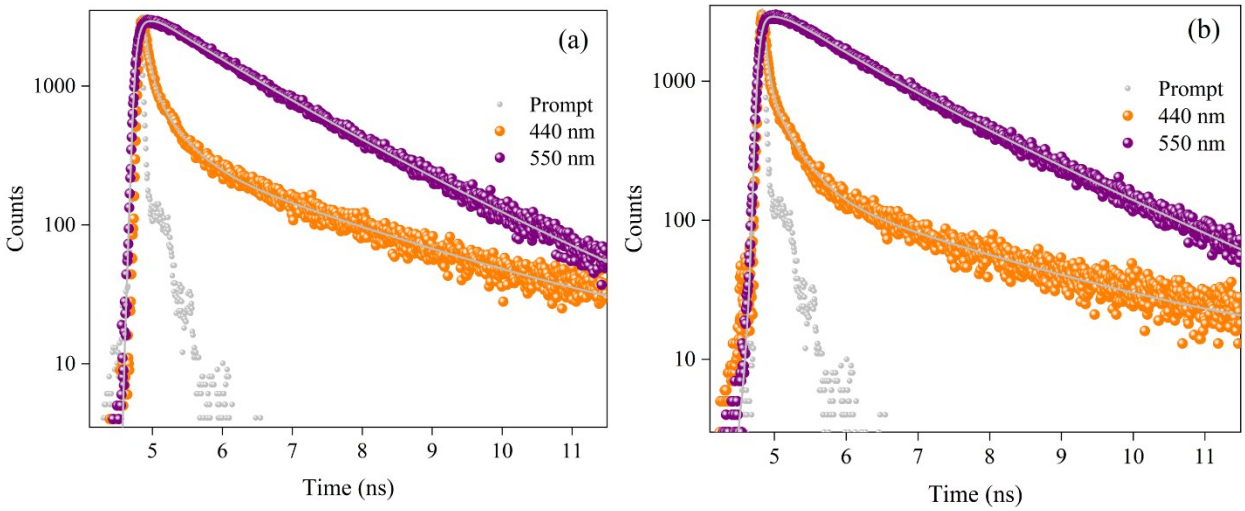

Figure S10. Lifetime decay profiles of 3HF in (a) Ia3d and (b) Pn3m LLC phases collected at different emission wavelengths. The solid lines denote the fits of the decay profiles.

Table S2. Lifetime fitting parameters of 3HF and FIS in neat solvents from femtosecond up-conversion experiments.

Sample	α_1	τ_1 (ps)	α_2	τ_2 (ps)
3HF in MeOH	- 0.48	15	0.52	200
3HF in CH_3CN	- 0.35	10	0.65	660
FIS in MeOH	- 0.40	13	0.60	300
FIS in CH_3CN	- 0.31	8	0.69	530

Table S3. Lifetime fitting parameters of FIS and 3HF in Water from TCSPC Experiments.

Sample	λ_{em}	α_1	τ_1 (ns)	α_2	τ_2 (ns)	α_3	τ_3 (ns)
3HF in water	550	0.99	0.170	0.01	3.781	-	-
FIS in water	550	0.09	1.045	0.74	0.050	0.17	0.325

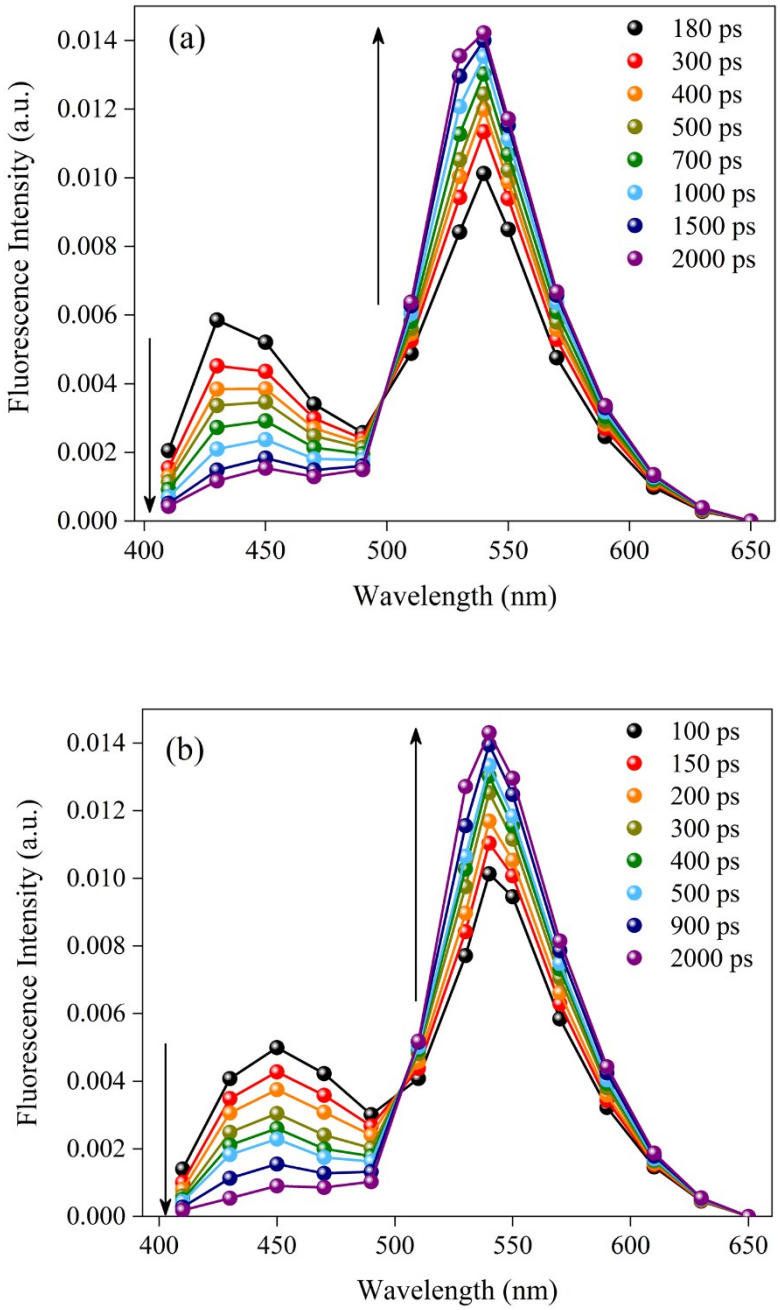

Figure S11. Time resolved area normalised spectra of FIS in (a) Ia3d and (b) Pn3m LLC phases.

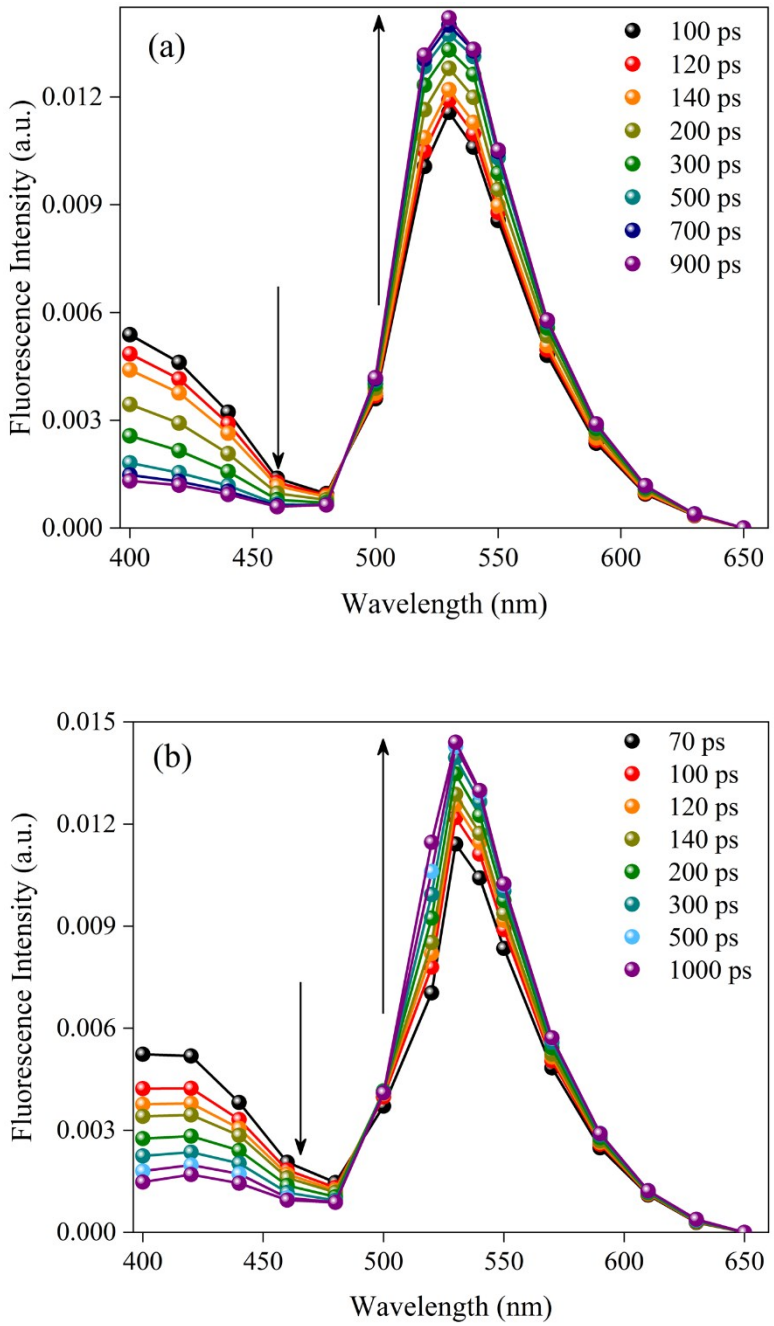

Figure S12. Time resolved area normalised spectra of 3HF in (a) Ia3d and (b) Pn3m LLC phases.

Computational Studies

In order to determine the ground state of the FIS (FIS: Water) molecule in gas (solvent) phase, we have performed DFT based calculations using the Gaussian Software (G09-rev-D).[3] We have used the B3LYP exchange-correlation functional[4] and double zeta basis set[5]. We find that the lowest energy structures of the FIS molecule are planar (Figure S12 a)). However FIS:Water lowest energy structures lost planarity and water molecule formed hydrogen bonded with hydroxyl group as shown in the following Figure S12 b). Here we defined proton transfer co-ordinate (δ), as the difference between non-covalent bond (d1) and O-H covalent bond (d2) of FIS molecule. Similarly, we defined another proton transfer co-ordinate (δ`), as the difference between non-covalent bond (D1) with hydrogen bonded water molecule in FIS:Water complex and O-H covalent bond (D2) of the molecule. We performed one dimensional (1D) potential energy profile of both important proton transfer coordinates (δ and δ`). The negative values of the proton transfer coordinate (PTC) would result in tautomers of the FIS molecule. We showed important optimised hydrogen bonding parameters in Figure S13 and Figure S14. Then further we compared with intrinsic co-ordinates (IRC) (Figure S16). Furthermore, excited state study performed by TDDFT and computed electron density difference map (EDDM) (Figure S15) of the first excited transition by Gauss-Sum package.[6] The EDDM profile shows charge transfer of FIS molecule.

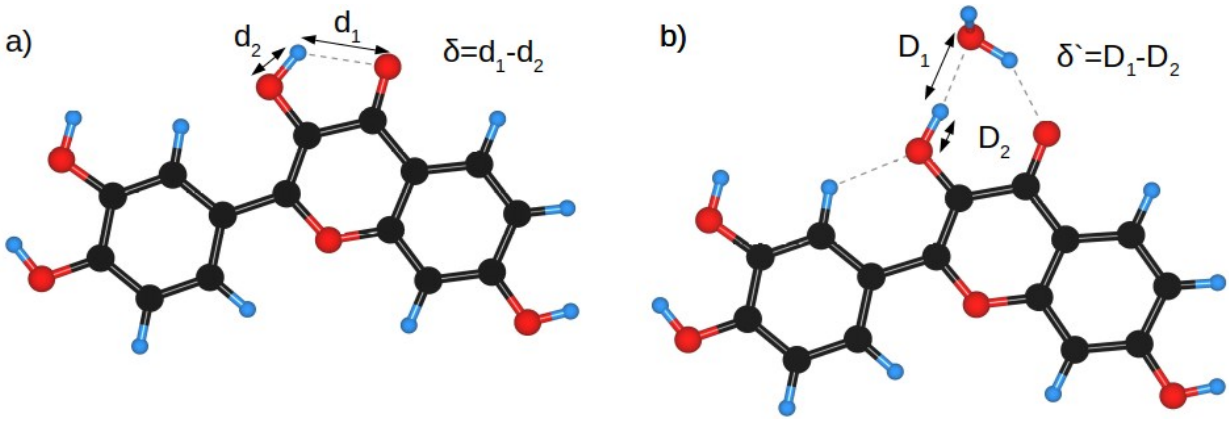

Figure S13. Optimized geometries of a) FIS molecule and b) FIS:Water complex.

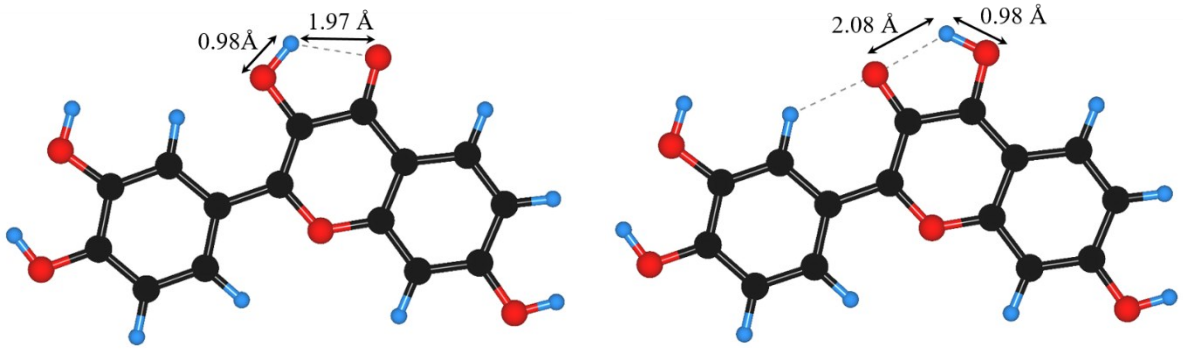

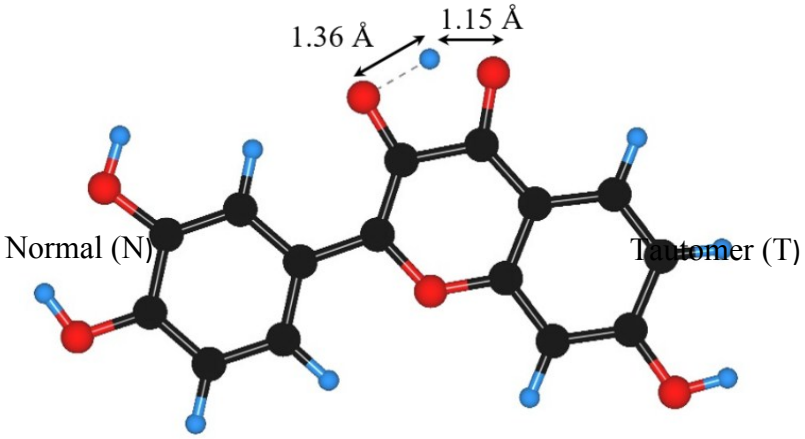

Transition State (T.S)

Figure S14. Optimized ground state molecular structures of the normal, tautomer and proton transfer transition state structures of FIS in gas phase. Bond distances are indicated with arrows.

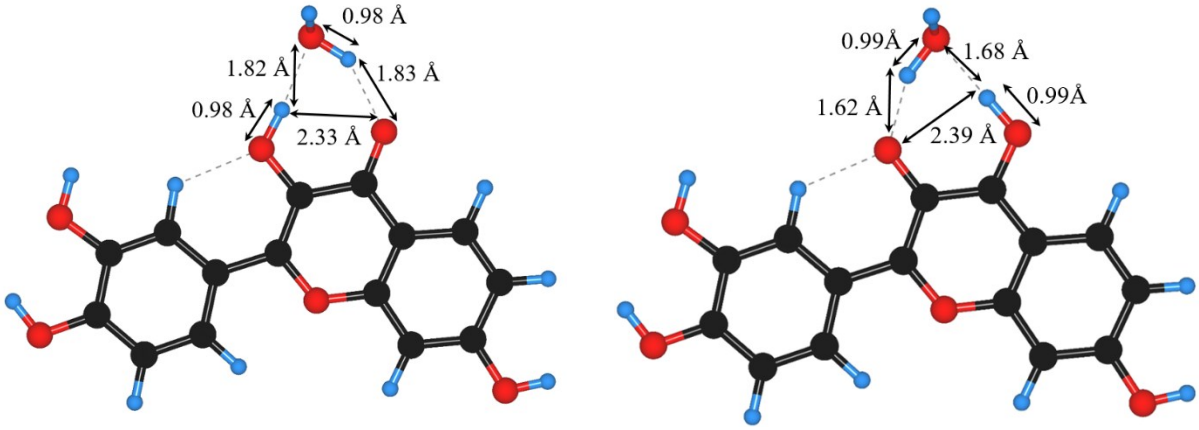

Normal (N) Tautomer (T)

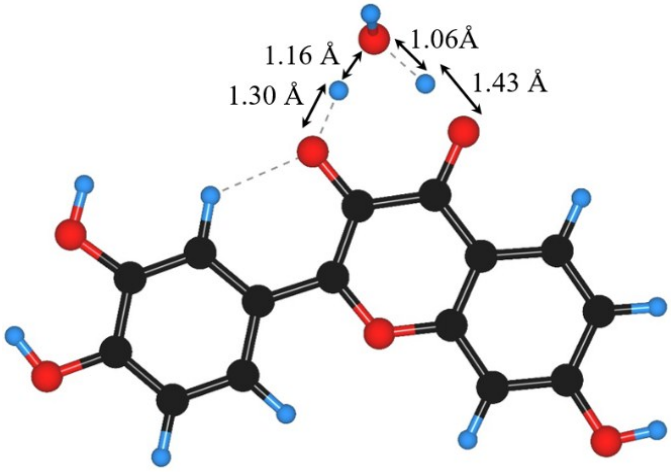

Transition State (T.S)

Figure S15. Optimized ground state molecular structures of the normal, tautomer and proton transfer transition state structures of FIS:Water complex. Bond distances are indicated with arrows.

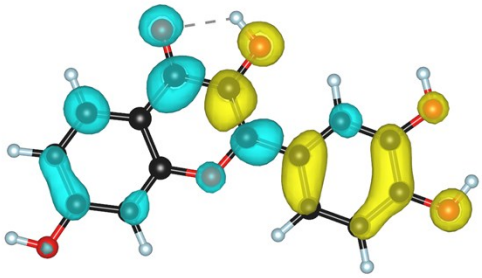

FIS Normal (N)

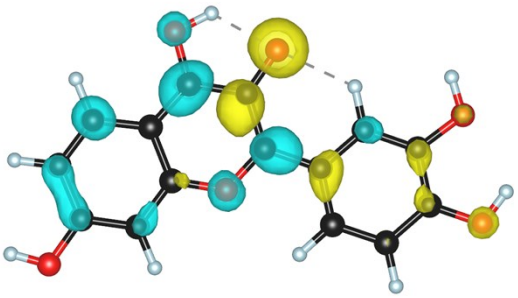

FIS Tautomer (T)

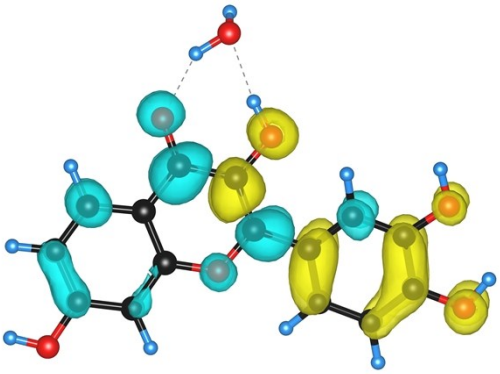

Normal form of FIS:Water Complex

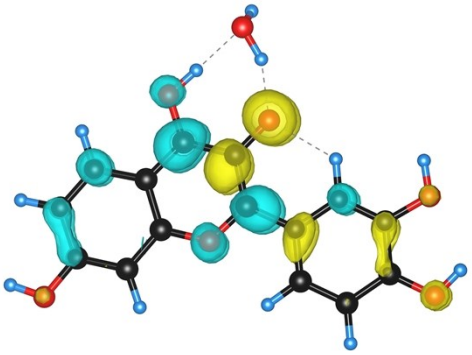

Tautomer form of FIS:Water Complex

Figure S16: Electron density difference maps (EDDM) of the normal and tautomer forms of FIS and the normal and tautomer forms of FIS:Water complexes. Hydrogen bonding is denoted by grey dashed lines.

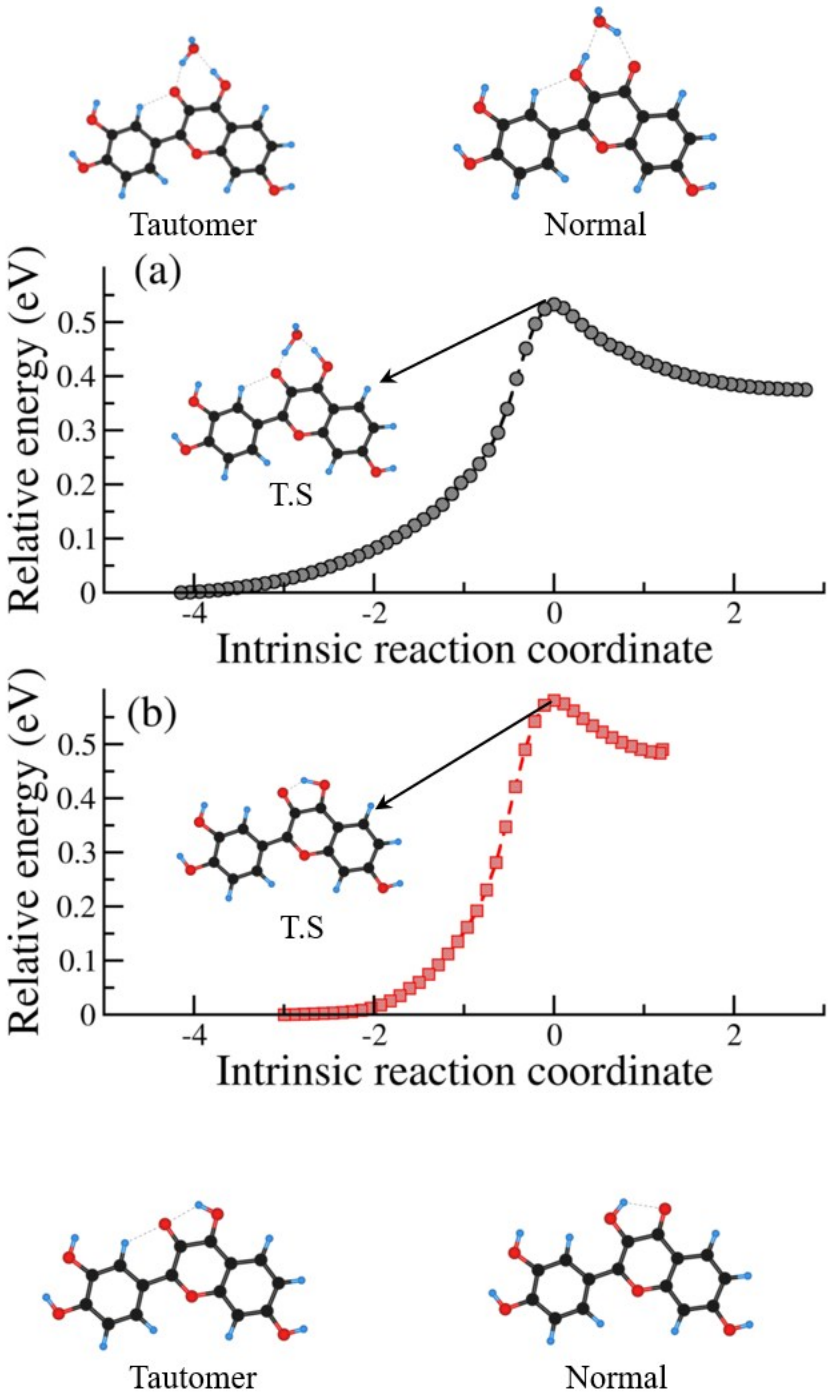

Figure S17: The intramolecular reaction coordinate (IRC) profile of (a) FIS:Water complex and (b) FIS along proton transfer coordinate.

References

1. Qiu, H.; Caffrey, M. Lyotropic and Thermotropic Phase Behavior of Hydrated Monoacylglycerols: Structure Characterization of Monovaccenin. J. Phys. Chem. B 1998, 102, 4819-4829.
2. Templer, R. H.; Seddon, J. M.; Warrender, N. A.; Syrykh, A.; Huang, Z.; Winter, R.; Erbes, J. Inverse Bicontinuous Cubic Phases in 2:1 Fatty Acid/Phosphatidylcholine Mixtures. The Effects of Chain Length, Hydration, and Temperature. J. Phys. Chem. B 1998, 102, 7251-7261.
3. M. J. Frisch, G. W. Trucks, H. B. Schlegel, G. E. Scuseria, M. A. Robb, J. R. Cheeseman, G. Scalmani, V. Barone, G. A. Petersson, H. Nakatsuji, X. Li, M. Caricato, A. V. Marenich, J. Bloino, B. G. Janesko, R. Gomperts, B. Mennucci, H. P. Hratchian, J. V. Ortiz, A. F. Izmaylov, J. L. Sonnenberg, Williams, F. Ding, F. Lipparini, F. Egidi, J. Goings, B. Peng, A. Petrone, T. Henderson, D. Ranasinghe, V. G. Zakrzewski, J. Gao, N. Rega, G. Zheng, W. Liang, M. Hada, M. Ehara, K. Toyota, R. Fukuda, J. Hasegawa, M. Ishida, T. Nakajima, Y. Honda, O. Kitao, H. Nakai, T. Vreven, K. Throssell, J. A. Montgomery Jr., J. E. Peralta, F. Ogliaro, M. J. Bearpark, J. J. Heyd, E. N. Brothers, K. N. Kudin, V. N. Staroverov, T. A. Keith, R. Kobayashi, J. Normand, K. Raghavachari, A. P. Rendell, J. C. Burant, S. S. Iyengar, J. Tomasi, M. Cossi, J. M. Millam, M. Klene, C. Adamo, R. Cammi, J. W. Ochterski, R. L. Martin, K. Morokuma, O. Farkas, J. B. Foresman and D. J. Fox, *Gaussian 16 Rev. C.01*, Wallingford, CT, 2016.
4. J. Tirado-Rives, W. L. Jorgensen, *J. Chem. Theory Comput.*, 2008, **4**, 297-306.
5. R. Krishnan, J. S. Binkley, R. Seeger, J. A. Pople, *J. Chem. Phys.*, 1980, **72**, 650-654.
6. N. M. O'boyle, A. L. Tenderholt, K. M. Langner, *J. Comput. Chem.*, 2008, **29**, 839-845.